Response properties in the adsorption–desorption model on a triangular lattice

J.R. Šćepanović [a], D. Stojiljković [a], Z.M. Jakšić [a], Lj. Budinski-Petković [b], S.B. Vrhovac [a],*

[a] *Scientific Computing Laboratory, Institute of Physics Belgrade, University of Belgrade, Pregrevica 118, Zemun 11080, Belgrade, Serbia*
[b] *Faculty of Engineering, University of Novi Sad, Trg D. Obradovića 6, Novi Sad 21000, Serbia*

HIGHLIGHTS

- Reversible RSA of objects of various shapes on a 2D triangular lattice is studied.
- We study the response of the model to an abrupt change in desorption probability.
- Short-time response strongly depends on the symmetry properties of the shapes.
- Density correlations decay slower for more symmetrical shapes.
- We observe the weakening of correlation features in multicomponent systems.

ARTICLE INFO

ABSTRACT

The out-of-equilibrium dynamical processes during the reversible random sequential adsorption (RSA) of objects of various shapes on a two-dimensional triangular lattice are studied numerically by means of Monte Carlo simulations. We focused on the influence of the order of symmetry axis of the shape on the response of the reversible RSA model to sudden perturbations of the desorption probability P_d. We provide a detailed discussion of the significance of collective events for governing the time coverage behavior of shapes with different rotational symmetries. We calculate the two-time density–density correlation function $C(t, t_w)$ for various waiting times t_w and show that longer memory of the initial state persists for the more symmetrical shapes. Our model displays nonequilibrium dynamical effects such as aging. We find that the correlation function $C(t, t_w)$ for all objects scales as a function of single variable $\ln(t_w)/\ln(t)$. We also study the short-term memory effects in two-component mixtures of extended objects and give a detailed analysis of the contribution to the densification kinetics coming from each mixture component. We observe the weakening of correlation features for the deposition processes in multicomponent systems.

© 2016 Elsevier B.V. All rights reserved.

1. Introduction

The understanding of random sequential adsorption (RSA) model has attracted large attention as a paradigmatic approach towards irreversibility, as well as due to the strong departure of the process from equilibrium behavior. In the RSA model [1], particles are added randomly and sequentially onto a substrate without overlapping each other. RSA model assumes that

---

deposited particles can neither diffuse along, nor desorb from the surface. The kinetic properties of a deposition process are described by the time evolution of the coverage $\theta(t)$, which is the fraction of the substrate area covered by the adsorbed particles. Within a monolayer deposit, each adsorbed particle affects the geometry of all later placements. Due to the blocking of the substrate area, at large times the coverage approaches the jammed-state value θ_J, where only gaps too small to fit new particles are left in the monolayer.

In pursuit of understanding the various aspects of the adsorption phenomenon large number of studies have taken place. A comprehensive survey on RSA and cooperative sequential adsorptions is given by Evans [2]. Other surveys include Privman [3–5], Cadilhe et al. [4], Senger et al. [6], and Talbot et al. [7].

In many real physical situations it is necessary to consider the possibility of desorption of deposited particles [8–10]. Adsorption–desorption processes are important in the binding of ions to a Langmuir monolayer [11], and in many catalytic reactions. Binding and unbinding of kinesin motors to microtubules [12], of myosin to actin filaments, and of proteins to DNA are commonly studied biological examples. Possibility of desorption makes the process reversible and the system ultimately reaches an equilibrium state when the rate of desorption events balances the rate of adsorption events. The kinetics of the reversible RSA is governed by the ratio of adsorption to desorption rate, $K = k_+/k_-$. For large values of K, there is a rapid approach to density $\theta \simeq \theta_J$, followed by a slow relaxation to a higher steady-state value θ_∞ [13–16].

The reversible RSA model is frequently used by many authors to reproduce qualitatively the densification kinetics and other features of weakly vibrated granular materials [9,17,10]. The phenomenon of granular compaction involves the increase of the density of a granular medium subjected to shaking or tapping [18–23]. The relaxation dynamics is extremely slow, taking many thousands of taps to approach the steady state, and it slows down for lower vibration intensities. The final steady-state density is a decreasing function of the vibration intensity [23]. Dynamics of the reversible RSA model depends on the excluded volume and geometrical frustration, just as in the case of granular compaction. This model can be regarded as a simple picture of a horizontal layer of a granular material, perpendicular to the tapping force. As a result of a tapping event, particles leave the layer at random and compaction proceeds when particles fall back into the layer under the influence of gravity. The ratio of desorption to adsorption rate $1/K = k_-/k_+$ within the model plays a role similar to the vibration intensity Γ in real experiments [24] (Γ is defined as the ratio of the peak acceleration of the tap to the gravitational acceleration g).

One of the striking features of granular materials are the memory effects observed by measuring the short-time response to an instantaneous change in the tapping acceleration Γ [25]. For a sudden decrease in Γ it was observed that on short-time scales the compaction rate increases, while for a sudden increase in Γ the system dilates for short times. This behavior is transient and after several taps there is a crossover to the "normal" behavior, with the relaxation rate becoming the same as in constant vibration intensity mode. Furthermore, Nicolas et al. [26] have also shown that periodic shear compaction exhibits a nontrivial response to a sudden change in shear amplitude. The rapid variation of volume fraction induced by the sudden change of shear angle is proportional and opposite to the angle change. The short-term memory effects observed in granular materials are reflected in the fact that the future evolution of the packing fraction θ after time t_w depends not only on the $\theta(t_w)$, but also on the previous tapping history. It is important to note that the parking lot model (PLM, 1D off-lattice reversible RSA model) [24,9,27,17] is a widely used model which can reproduce qualitatively the short-term memory effects of a weakly vibrated granular material. In Ref. [10] we have presented the detailed studies of the short-term memory effects in the framework of a two-dimensional reversible RSA model on a square lattice.

An important issue in two-dimensional deposition is the influence of the shape of the adsorbed particle. It is well known that the size, aspect ratio and symmetry properties of the object have a significant role in the processes of both irreversible and reversible deposition. The numerical analyses for the irreversible deposition of various shapes and their mixtures on a triangular lattice [28,29] establish that the approach to the jamming limit follows the exponential law with the rate dependent mostly on the order of symmetry axis of the shape. In the reversible case of deposition on a triangular lattice [15,30], we have found that the coverage kinetics is severely slowed down with the increase of the order of symmetry of the shape.

The main goal of the present study is to investigate the interplay between the response of the reversible RSA model to sudden perturbations of the desorption probability P_d and the symmetry properties of deposited shapes. Numerical simulations of adsorption–desorption processes are performed for various shapes on the triangular lattice, shown in Table 1. These shapes are made of self-avoiding walks of the same length $\ell = 2$, but they differ in their symmetry properties. The response in the evolution of the density $\theta(t)$ to a change in the desorption probability P_d at a given time t_w is accompanied by transformation of the local configurations in the covering. Essentially, collective (two-particle) events are responsible for the evolution of θ for $\theta > \theta_J$. Size of the objects and their symmetry properties have a significant influence on these collective events, thus affecting the kinetics of the deposition process [15,31,30]. Since we focus our interest on the influence of symmetry of the object on the response of the system to sudden perturbation of the desorption probability P_d, it is necessary to analyze the processes with the objects of the same size. In this paper we also study the response of two-component mixtures of extended objects (see, Table 1) to sudden perturbations of the desorption probability P_d. We did carry out a detailed analysis of the contribution to the densification kinetics coming from each mixture component. Finally, we study the nonequilibrium two-time density–density correlation function $C(t, t_w)$. We focus, in particular, on the influence of symmetry properties of the shapes on the decay of $C(t, t_w)$ and aging effects. This work provides for the first time the link between the short-term memory effects and intrinsic properties of the shapes.

Recently, we have analyzed the growth of the coverage $\theta(t)$ above the jamming limit to its steady-state value θ_∞ within the framework of the adsorption–desorption model of dimers in one dimension [32]. We reported a numerical evidence

Table 1

Various shapes (x) of length $\ell^{(x)} = 2$ on a triangular lattice. Here $n_s^{(x)}$ denotes the order of the symmetry axis of the shape (x), $s^{(x)}$ is the object size, and $\theta_J^{(x)}$ is the jamming coverage. The numbers in parentheses are the numerical values of the standard uncertainty of $\theta_J^{(x)}$ referred to the last digits of the quoted value.

(x)	Shape	$n_s^{(x)}$	$s^{(x)}$	$\ell^{(x)}$	$\theta_J^{(x)}$
(A)		2	2		0.8362(4)
(B)		1	1.5	2	0.8345(5)
(C)		3	1		0.7970(4)

that the time needed for a system to reach the given coverage θ can be significantly reduced if P_d decreases both stepwise and linearly (continuously) over a certain time domain. Based on the results in the present paper, one would expect that the growth of the coverage in the case of the two-dimensional reversible RSA model can also be accelerated by decreasing the desorption rate during the deposition process. However, our results indicate that the efficiency of this process depends on the symmetry properties of the deposited objects. This must be taken into account when developing an optimal protocol which significantly hastens the process for achieving high coverage densities.

The paper is organized as follows. Section 2 describes the details of the simulations. We give the simulation results and discussions in Section 3. Finally, Section 4 contains some additional comments and final remarks.

2. Definition of the model and numerical simulation

The depositing shapes are modeled by directed self-avoiding walks on a triangular lattice. A self-avoiding shape of length ℓ is a sequence of distinct vertices $(\omega_0, \ldots, \omega_l)$ such that each vertex is a nearest neighbor of its predecessor. Consequently, a walk of length ℓ covers $\ell + 1$ lattice sites. On a triangular lattice objects with a symmetry axis of first, second, third, and sixth order can be formed. Rotational symmetry of order n_s, also called n-fold rotational symmetry, with respect to a particular axis perpendicular to the triangular lattice, means that rotation by an angle of $2\pi/n_s$ does not change the object. In Table 1 three different shapes that can be made by self-avoiding walks of length $\ell = 2$ are shown. It should be noted that size s of an object is taken as the greatest projection of the walk that makes the object on one of the six directions. Thus the size of a dot is $s = 0$, the size of a one-step walk is $s = 1$, and for example the size of the second object (B) in Table 1 is $s = 1.5$ in lattice spacing.

The Monte Carlo simulations are performed on a triangular lattice of size $L^2 = 120 \times 120$. At each Monte Carlo step adsorption is attempted with probability P_a and desorption with probability P_d. In the simulations of deposition processes with desorption, the kinetics is governed by the desorption to adsorption probability ratio $\Gamma = P_d/P_a$ [33,34]. Since we are interested in the ratio Γ, in order to save computer time, it is convenient to take the adsorption probability to be $P_a = 1$, i.e., to try an adsorption at each Monte Carlo step.

We start with an initially empty triangular lattice. Adsorption and desorption processes perform simultaneously with corresponding probabilities. For each of these processes, a lattice site is chosen at random. In the case of adsorption, we attempt to place the object with the beginning at the selected site. If the selected site is unoccupied, one of the six possible orientations is chosen at random and deposition of the object is tried in that direction. We fix the beginning of the walk that makes the shape of length ℓ at the selected site and search whether all successive ℓ sites are unoccupied. If they are empty, we occupy these $\ell + 1$ sites and place the object. If, however, any of the ℓ sites are already occupied, the deposition attempt is rejected and the configuration remains unchanged. This scheme is usually called conventional or standard model of deposition. The other strategy to perform an RSA, where we check all possible directions from the selected site, is named the end-on model [28]. On the other hand, if the attempted process is desorption and if the selected site is already occupied by a previously adsorbed object, the object is removed with probability P_d from the layer.

Adsorption–desorption processes on discrete substrates display a surprisingly complex kinetics [9,35]. Here we consider the case of rapid adsorption and slow desorption ($\Gamma = P_d/P_a \ll 1$). Then there exist two time scales controlling the evolution of the coverage $\theta(t)$. The first stage of the process is dominated by adsorption events and the kinetics displays an RSA-like behavior. With the growth of the coverage the desorption process becomes more and more important. Increasing the coverage over the jamming limit is possible only due to the collective rearrangement of the adsorbed particles in order to open a hole large enough for the adsorption of an additional particle. We are interested in the approach to the equilibrium coverage in this later, post-jamming time range.

Periodic boundary conditions are used in all directions. The time t is counted by the number of adsorption attempts and scaled by the total number of lattice sites L^2. The data are averaged over 10^3 independent runs for each shape and each desorption probability. The finite-size effects, which are generally weak, can be neglected for object sizes $<L/8$ [36].

Furthermore, during the simulation of irreversible deposition we record the number of inaccessible sites in the lattice. A site is inaccessible if it is occupied or it cannot be the beginning of the shape. The jamming limit θ_J is reached when the number of inaccessible sites is equal to the total number of lattice sites. Values of jamming coverages $\theta_J^{(x)}$ for three objects $(x) \in \{(A), (B), (C)\}$ of length $\ell = 2$ are given in Table 1. Fig. 1 shows a typical snapshot configuration at coverage fraction $\theta = 0.89$ obtained in the case of $P_d = 0.0045$ for line-segments of length $\ell = 2$ (object (A) from Table 1).
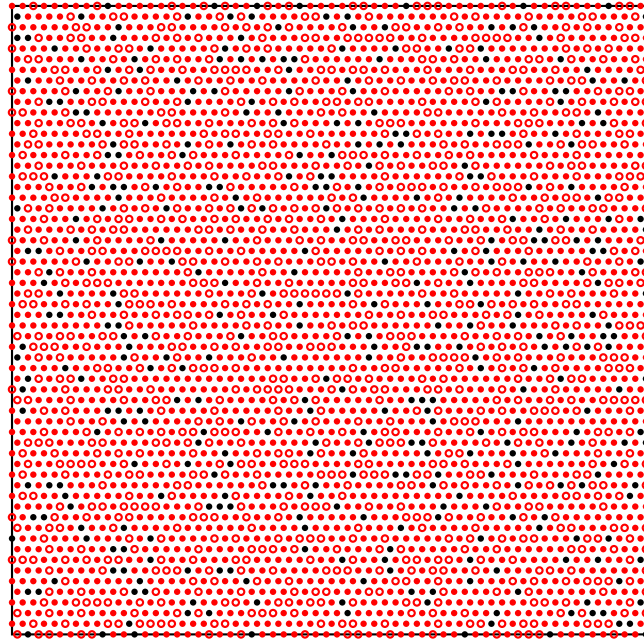
Fig. 1. Snapshot of pattern formed during the reversible deposition of object (A) from Table 1 correspond to coverage fraction $\theta = 0.89$, and $P_d = 0.0045$. Nodes of the grid corresponding to the beginning of the walk that makes the shape are indicated by large open points. Empty nodes are marked with black points. A lattice of size $L^2 = 60 \times 60$ is used.

3. Results and discussion

In order to analyze the response of the reversible RSA model to sudden perturbations of the desorption probability P_d, we have carried out series of Monte Carlo simulations for objects (A), (B), and (C), all of them starting from an empty lattice. The system was evolved at a fixed desorption probability $P_d^{(1)}$. At a certain time, t_w, the value of the desorption probability $P_d^{(1)}$ was instantaneously changed to another value $P_d^{(2)}$. The variations of coverage $\theta(t)$ in the case of object (A), for three different values of t_w are reported in Fig. 2. It must be emphasized that the same kind of numerical experiments for objects (B) and (C) produce qualitatively similar results for the time evolution of the coverage $\theta(t)$. First, in Fig. 2 we show the response of the system to the desorption probability shift from $P_d^{(1)} = 0.0045$ to $P_d^{(2)} = 0.0015$ at the times $t_w = 139, 205, 307$ needed for a system to reach the coverages $\theta_w = 0.87, 0.88, 0.89$, respectively, in the process of reversible RSA with $P_d^{(1)} = 0.0045$. As it can be seen, when $P_d^{(1)} > P_d^{(2)}$, the compaction rate of the perturbed system first increases on short-time scales. After a transient, compaction slows down and the rate of compaction crosses over to the one observed at constant desorption probability $P_d^{(2)}$.

Fig. 2 also shows typical response of the system at short times after an abrupt change of the desorption probability from $P_d^{(1)} = 0.0015$ to $P_d^{(2)} = 0.0045$ at the times $t_w = 304, 441, 639$ needed for a system to reach the coverages $\theta_w = 0.87, 0.88, 0.89$, respectively, in the process of reversible RSA with $P_d^{(1)} = 0.0015$. For $P_d^{(1)} < P_d^{(2)}$ we find a short-term response of the system opposite to the previous case. First, as the desorption probability is increased, one observes a decompaction. Later on, the larger desorption probability $P_d^{(2)}$ begins to prevail and the compaction proceeds faster, at the normal rate for constant $P_d^{(2)}$. In addition, the comparison (not shown here) of the density relaxations $\theta(t)$ at various changes in the desorption probability P_d indicates that the amplitude of the jump in the compaction rate is larger for larger jump of the desorption probability $\Delta P_d = |P_d^{(2)} - P_d^{(1)}|$. The probabilities of $P_d^{(1)} = 0.0015$ and $P_d^{(2)} = 0.0045$ are chosen to provide a wide density range $\theta \in (0.86, 0.89)$ for all three objects where desorption probability can be abruptly changed. We have verified that usage of different, but sufficiently small, values of desorption probabilities $P_d^{(1)}$ and $P_d^{(2)}$ gives quantitatively similar results leading to qualitatively same phenomenology.

This shows that the system has some memory of its history at t_w. Memory effect implies that the system can be found in states, characterized by the same coverage fraction θ, that evolve differently under further reversible deposition with the same desorption probability P_d [17]. This is illustrated in the inset of Fig. 2. The points M and N correspond to states with equal coverage fraction $\theta_c = 0.8686$, equal value of $P_d = 0.0045$, but different further evolution. Their responses to the same desorption probability P_d are different: covering M becomes looser whereas covering N pursues its compaction. In other words, the density evolution $\theta(t)$ after the points M and N depends not only on the density θ_c, but also on the previous tapping history. The memory of the history up to the density θ_c is encoded in the arrangement of the objects in the covering.
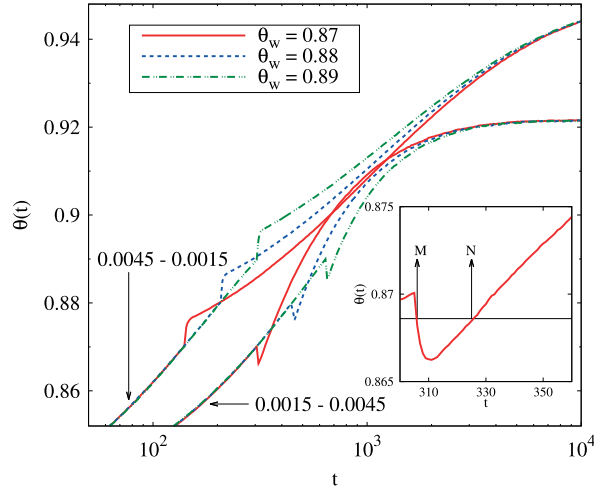
Fig. 2. Time evolution of the coverage $\theta(t)$ for object (A) when the desorption probability is changed from $P_d^{(1)} = 0.0045$ to $P_d^{(2)} = 0.0015$ (from $P_d^{(1)} = 0.0015$ to $P_d^{(2)} = 0.0045$) at times $t_w = 139, 205, 307$ ($t_w = 304, 441, 639$) needed for the system to reach the coverages $\theta_w = 0.87, 0.88, 0.89$, respectively, in the process of reversible RSA with $P_d^{(1)} = 0.0045$ ($P_d^{(1)} = 0.0015$). Inset: Zoom up on the region around $t_w = 304$ ($\theta(t_w) = 0.87$) when the desorption probability switches from $P_d^{(1)} = 0.0015$ to $P_d^{(2)} = 0.0045$. The points M and N correspond to states with equal density $\theta_c = 0.8686$, equal value of $P_d^{(2)} = 0.0045$, but different further evolution.

Interpretation of these results for all objects (A), (B), and (C) is quite straightforward using the results of Refs. [37,9,34]. The compaction rate just before t_w is determined by the desorption probability $P_d(t_w - 0)$ and by the fraction of the substrate, $\Phi(t_w - 0)$, that is available for the insertion of a new particle. The quantity $\Phi(t_w - 0)$ (the insertion probability) strongly depends on the state of the system, but it is not unambiguously determined by the coverage fraction $\theta(t_w - 0)$ at the same instant [9,10]. When P_d is abruptly lowered, the first effect is that the particles tend to decrease the fraction of the substrate that is available for deposition of new particles, and the layer becomes more compact. Therefore the rate of compaction first increases with respect to the unperturbed case. At larger times, however, the compaction is slowed down by the creation of a denser substrate and smaller fraction of the layer that is available for the insertion of a new particle.

When the desorption probability P_d is suddenly increased at t_w, the first effect is decompaction. On short-time scales, the interplay between the insertion probability and desorption probability leads to the fast density changes. During this transient stage the fraction of the substrate that is available for the insertion of a new particle is an increasing function of time. After this transient interval, the adsorption events prevail, and the compaction proceeds faster. Growing of the insertion probability, $\Phi(t)$, during the transient time, leads to the more efficient densification afterwards.

Here we focus our interest on the influence of the order of symmetry axis of the shape on the response of the reversible RSA model to sudden perturbation of the desorption probability P_d. Consequently, we considered series of numerical experiments where the short-term memory effects were analyzed for the three systems. In this set of experiments the objects (A), (B), and (C) were deposited to the same density θ_w with desorption probability $P_d^{(1)}$. After the density θ_w was achieved, desorption probability P_d was switched from $P_d^{(1)}$ to $P_d^{(2)}$ ($P_d^{(2)} \leqslant P_d^{(1)}$). In Fig. 3 we show the time evolution of the density $\theta(t)$ during the deposition of objects (A), (B), and (C), when the desorption probability P_d is changed from $P_d^{(1)} = 0.0045$ to $P_d^{(2)} = 0.0015$. Here, the results for three different values of θ_w are reported, namely, 0.87, 0.88, and 0.89. The time origin for each experiment has been taken at the time when the system reached the prescribed density θ_w. In Fig. 4 the same set of numerical experiments is carried out, with the only difference that in this case the desorption probability is changed from $P_d^{(1)} = 0.0015$ to $P_d^{(2)} = 0.0045$. These simulations show that the short-time response to an instantaneous change in desorption probability P_d strongly depends on the symmetry properties of the shapes. From Figs. 3 and 4, it follows that the change in the compaction rate on short-time scales is less pronounced as order of symmetry axis of the shape n_s increases.

Qualitative interpretation of these results can be attained by exploiting the mechanism of collective events for governing the late-time changes in the coverage fraction ($\theta(t) > \theta_J$). In the following, we restrict ourselves to the case of weak desorption (large values of $K = P_a/P_d$), when the system of adsorbed particles evolves continuously toward an equilibrium disordered state. When a value of θ_J is reached, the rare desorption events are generally followed by immediate readsorption. The total number of particles is not changed by these *single* particle events. Essentially, collective events are responsible for the evolution of coverage fraction θ above the jamming limit θ_J. The rearrangement of state corresponding to $\theta > \theta_J$, to its steady-state value θ_∞, is dominated by the following *two-particle* processes:

(a) in one process ("$2 \rightarrow 1$"), responsible for decreasing the number of deposited objects by 1, two adjacent objects leave and a single one comes in their stead;
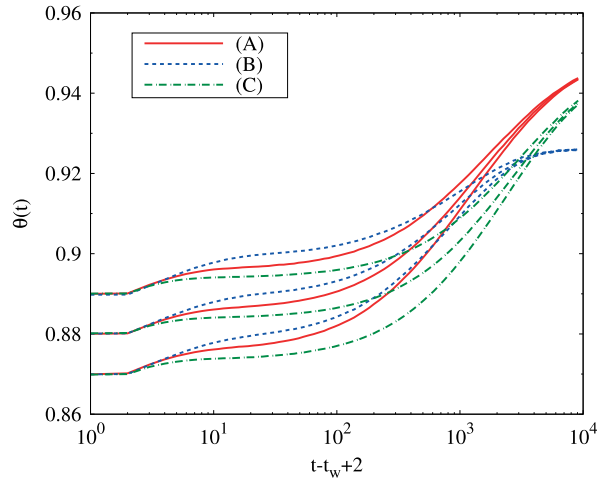
Fig. 3. Time evolution of the coverage $\theta(t)$ for objects (A), (B), and (C) when the desorption probability is changed from $P_d^{(1)} = 0.0045$ to $P_d^{(2)} = 0.0015$ at the times t_w needed for the system to reach the coverages $\theta_w = 0.87, 0.88, 0.89$ in the process of reversible RSA with $P_d^{(1)} = 0.0045$. The time origin for each experiment has been taken at the time when the system reached the prescribed density θ_w.
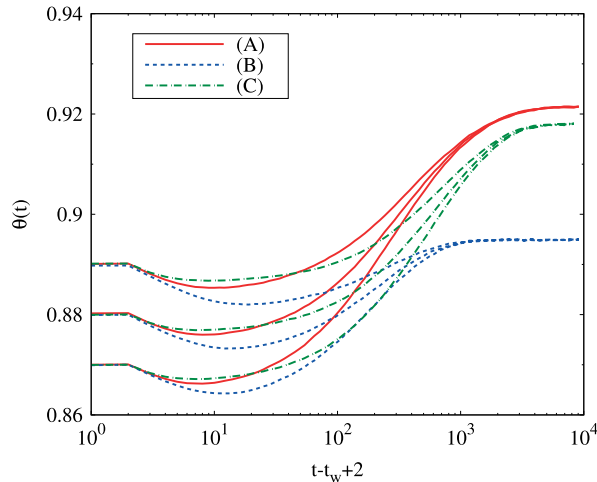
Fig. 4. Time evolution of the coverage $\theta(t)$ for objects (A), (B), and (C) when the desorption probability is changed from $P_d^{(1)} = 0.0015$ to $P_d^{(2)} = 0.0045$ at the times t_w needed for the system to reach the coverages $\theta_w = 0.87, 0.88, 0.89$ in the process of reversible RSA with $P_d^{(1)} = 0.0015$. The time origin for each experiment has been taken at the time when the system reached the prescribed density θ_w.

(b) the opposite process ("1 $\rightarrow$ 2") results in adding an extra object to the lattice: an object exits and leaves a space big enough for two objects.

The rate of the "2 $\rightarrow$ 1" process has three contributions. First, an object must leave the lattice. Then, an adjacent object must leave before the hole left by the first object fills. Finally, the big hole must be blocked by a badly sited object. In the opposite, "1 $\rightarrow$ 2" process, the void left by the object must be large enough for two objects. Note that the first incoming object must park with a sufficient precision in order to leave enough space for the second object.

It is obvious that the process "1 $\rightarrow$ 2" has an overall rate proportional to P_d ($P_d < 1$). Since the process "2 $\rightarrow$ 1" includes *two* consecutive desorption events, it is plausible that its overall rate is proportional to $(P_d)^2 < P_d < 1$. That is the main reason why, for coverages that are not close to the steady-state value, the collective event "1 $\rightarrow$ 2" is more frequent than the opposite event "2 $\rightarrow$ 1". This regime persists until the coverage is very close to the equilibrium value. Since the coverage fraction $\theta(t)$ increases and the available surface function Φ decreases, the overall rate at which the density increases is progressively reduced. The efficiency of desorption relative to adsorption increases, and the process reaches a steady state in which the rate of the "2 $\rightarrow$ 1" process is balanced by the "1 $\rightarrow$ 2" process.

Note that in Ref. Kolan et al. [24], the authors calculated the transition rates for the collective processes "1 $\rightleftarrows$ 2" in the case of a 1D RSA model and found that these rates account for the additional slow time scales. Ghaskadvi and Dennin [11] directly monitored the transition rates for the two-particle processes "1 $\rightleftarrows$ 2" as part of the simulation. They have directly confirmed the importance of multiparticle transitions "1 $\rightleftarrows$ 2" for governing the late time behavior of the system.
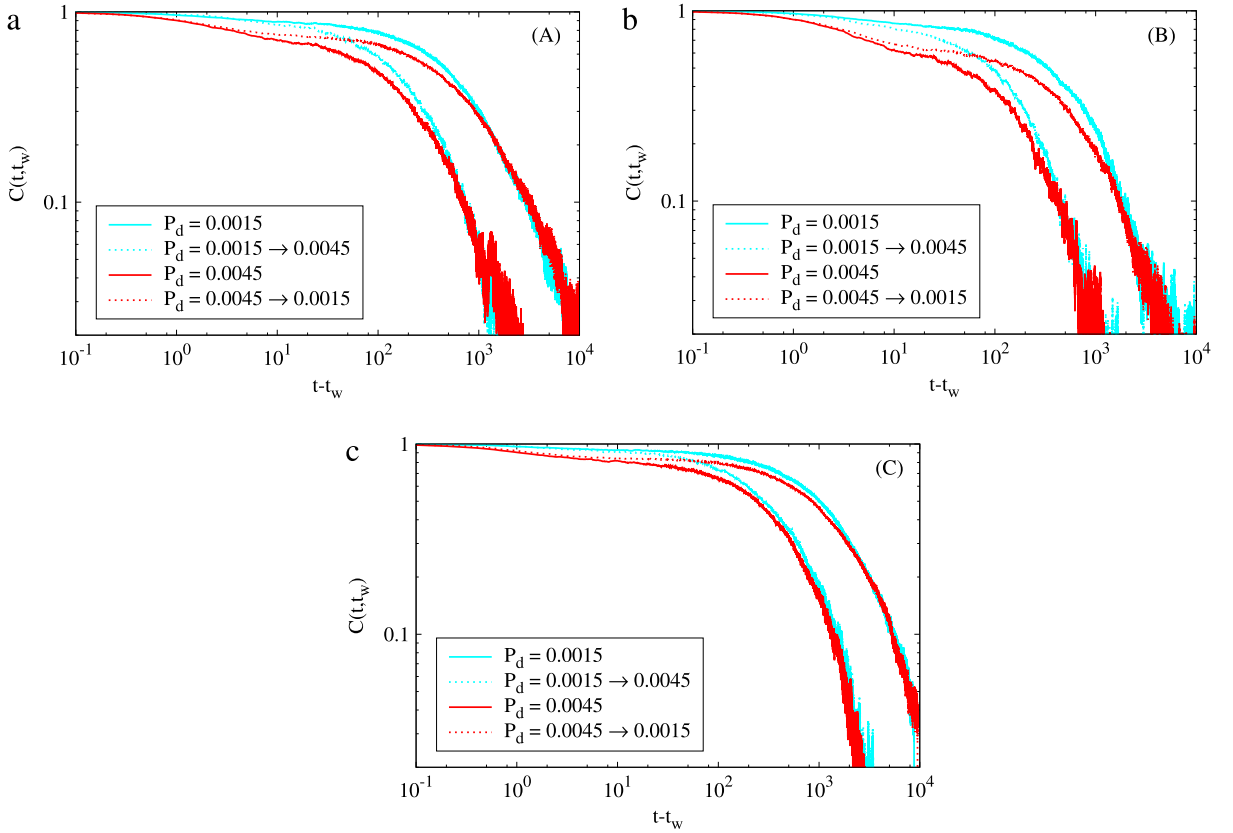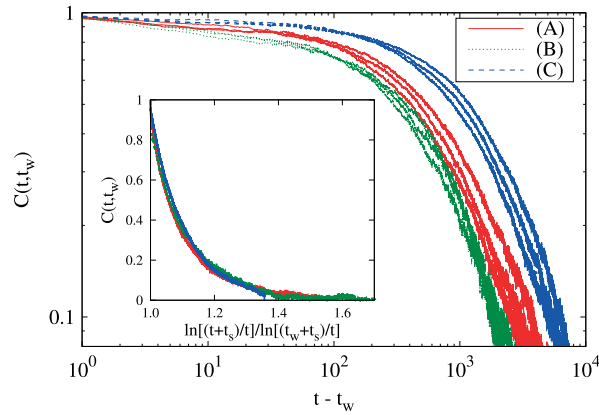
Fig. 5. Two-time density–density correlation function $C(t, t_w)$ for objects (a) (A), (b) (B), and (c) (C), as a function of $t - t_w$. The waiting time t_w corresponds to the time needed for the system to reach the coverage $\theta_w = 0.88$. The solid lines represent the temporal behavior of $C(t, t_w)$ obtained for the fixed desorption probabilities $P_d = 0.0015, 0.0045$, as indicated in the legend. The dashed lines represent the temporal dependence of $C(t, t_w)$ obtained from the runs during which an abrupt change of desorption probability $P_d^{(1)} = 0.0045 \rightarrow P_d^{(2)} = 0.0015$ ($P_d^{(1)} = 0.0015 \rightarrow P_d^{(2)} = 0.0045$) occurs at instant t_w, as indicated in the legend.

Now we try to explain how the order of symmetry axis of the shape changes the dynamics of the collective processes. Symmetry properties of the shapes have a significant influence on the filling of small isolated targets on the lattice. Indeed, there is only a restricted number of possible orientations in which an object can reach a previously opened location, provided the location is small enough. A shape with a symmetry axis of higher order has a greater number of possible orientations for deposition into small isolated locations on the lattice, and therefore enhanced probability of single-particle readsorption. This extends the mean waiting time between consecutive two-particle events "1 → 2", responsible for the density growth above θ_J, and causes a slowing down of the density growth. On the contrary, for the asymmetrical shapes (angled objects) there is a greater probability for blocking the neighboring sites. The noticeable drop in the probability of single-particle readsorption for the asymmetrical shapes is thus a clear consequence of the enhanced frustration of the spatial adsorption. Therefore, desorption process effectively opens holes that are large enough for insertion of two or more particles. This reduces the mean waiting time between consecutive multiparticle events which leads to more rapid growth of the density. When P_d is abruptly lowered, such a different object view is the cause of the enhanced density growth in the case of asymmetrical shapes as compared to those in the case of more round (symmetric) shapes. When the desorption probability P_d is suddenly increased, decompaction rate of the perturbed system on short-time scales is larger for shapes with a symmetry axis of lower order (Fig. 4). This is a consequence of the fact that unlike for the more symmetrical objects, much less orientations are allowed for irregular and asymmetric shapes falling in the isolated selective target spaces.

Below we try to further quantitatively characterize the out-of equilibrium dynamics in our system. Specifically, we have evaluated the two-time density–density correlation function, $C(t, t_w)$, and qualitatively analyzed its dependence on symmetry properties of the shapes. The normalized two-time density–density correlation function is defined as follows,

$$C(t, t_w) = \frac{\langle \theta(t)\theta(t_w) \rangle - \langle \theta(t) \rangle \langle \theta(t_w) \rangle}{\langle \theta^2(t_w) \rangle - \langle \theta(t_w) \rangle^2}, \quad t \geq t_w, \tag{1}$$

Fig. 6. Two-time density–density correlation function $C(t, t_w)$ for objects (A), (B), and (C), as a function of $t - t_w$. The waiting times t_w for each object correspond to the time needed for the system to reach the coverages $\theta_w = 0.87, 0.88, 0.89$ in the process of reversible RSA with $P_d = 0.0015$. The aging behavior is evident. Inset: The correlation $C(t, t_0)$ as a function of the scaling variable $\alpha = \ln[(t_0 + t_s)/\tau]/\ln[(t + t_s)/\tau]$. Fitting parameters are $t_s = 1760$, and $\tau(A) = 81$, $\tau(B) = 210$, $\tau(C) = 43$.
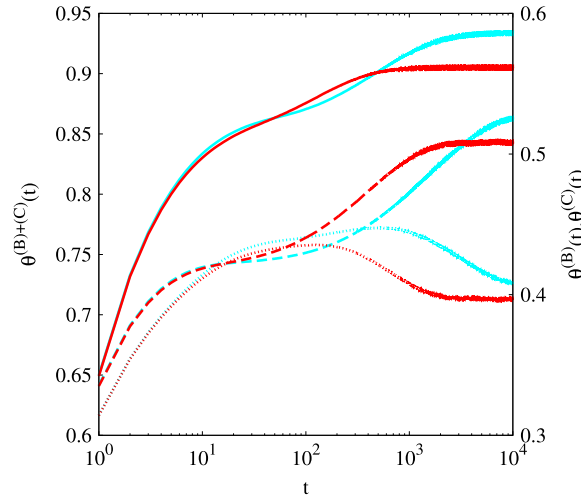

Fig. 7. Shown here is the time dependence of the coverage fraction $\theta^{(B)+(C)}$ for the mixture (B) + (C) and its components for two different values of desorption probability, $P_d = 0.0015, 0.0045$. Black (red) and grey (light blue) lines represent the results obtained for $P_d = 0.0045$ and $P_d = 0.0015$, respectively. The solid lines represent the temporal behavior of the coverage fraction $\theta^{(B)+(C)}(t)$ (left-hand axis). The dashed and dotted lines are plotted against the right-hand axis and give the coverage fraction versus time t of the component shapes (C), $\theta^{(C)}(t)$ (dashed), and (B), $\theta^{(B)}(t)$ (dotted). (For interpretation of the references to color in this figure legend, the reader is referred to the web version of this article.)

where the angular brackets $\langle \cdots \rangle$ denote an average over independent runs. In order to obtain reasonable statistics, it is necessary to average over many independent runs (typically 10^4). Out of equilibrium, $C(t, t_w)$ is a function of both times, t and t_w.

In Fig. 5 we show the behavior of the correlation function $C(t, t_w)$ for objects (A), (B), and (C). The waiting time t_w corresponds to the time needed for a system to reach the coverage $\theta_w = 0.88$. Numerical simulations for other densities, $\theta_w = 0.87, 0.89$, produce qualitatively similar results for the time evolution of the correlation function $C(t, t_w)$. In each plot of Fig. 5, the temporal dependence of $C(t, t_w)$ is displayed for the fixed desorption probabilities, $P_d = 0.0015, 0.0045$. For comparison, we also show the temporal dependence of $C(t, t_w)$ calculated from 10^4 independent runs during which an abrupt change of desorption probability $P_d^{(1)} = 0.0045 \to P_d^{(2)} = 0.0015$ ($P_d^{(1)} = 0.0015 \to P_d^{(2)} = 0.0045$) occurs at instant t_w. Correlation function obtained from the numerical simulation in which there is an instantaneous change of desorption probability $P_d^{(1)} \to P_d^{(2)}$, interpolates between two correlation functions calculated for constant desorption probabilities $P_d^{(1)}$ and $P_d^{(2)}$. At short times, this correlation function behaves as $C(t, t_w)$ obtained in the case when the desorption probability has the constant value $P_d^{(1)} = 0.0045$ ($P_d^{(1)} = 0.0015$). However, its long time behavior is consistent with the decay of $C(t, t_w)$ obtained in the case when the desorption probability has the constant value $P_d^{(2)} = 0.0015$ ($P_d^{(2)} = 0.0045$). By comparing the three panels in Fig. 5, it is obvious that global properties of the correlation function $C(t, t_w)$ of the density fluctuations depend on the order of symmetry axis of the shape n_s: as n_s grows, the correlation decays slower. In
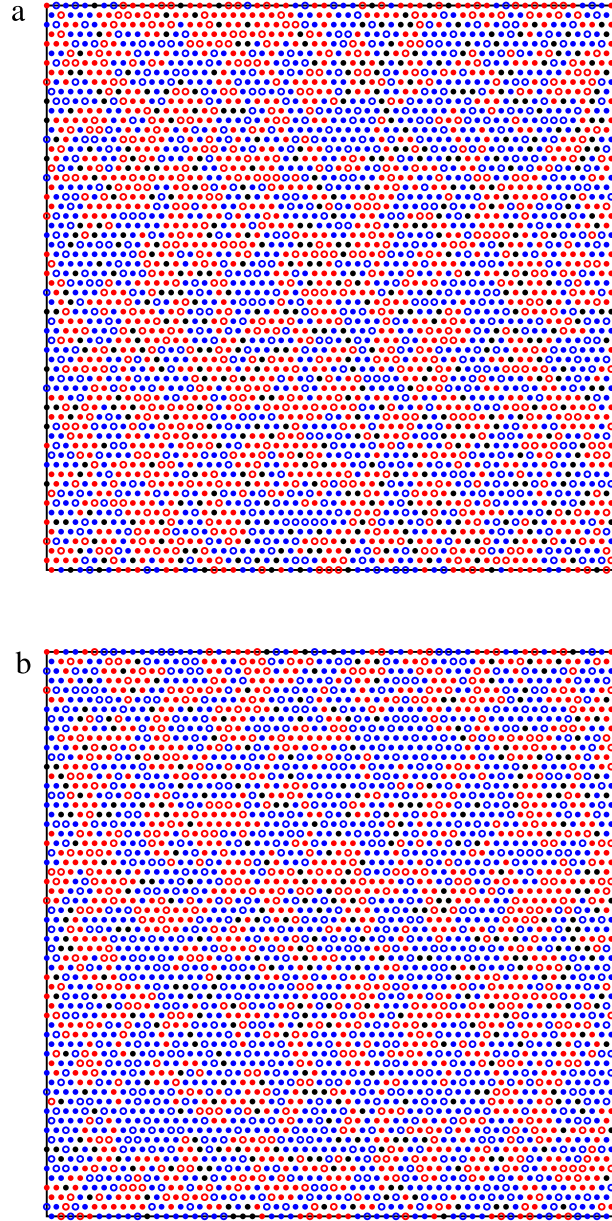
Fig. 8. Snapshot of pattern formed during the reversible deposition of mixture $(B)+(C)$ ((B)-red, (C)-blue) from Table 1 correspond to (a) coverage fraction $\theta^{(B)+(C)} = 0.88$, and (b) steady-state coverage $\theta^{(B)+(C)}_\infty = 0.9066$. Nodes of the grid corresponding to the beginning of the walk that makes the shapes are indicated by large open points. Empty nodes are marked with black points. A lattice of size $L^2 = 60 \times 60$ and $P_d = 0.0045$ are used. (For interpretation of the references to color in this figure legend, the reader is referred to the web version of this article.)

other words, longer memory of the initial state persists for the more symmetrical shapes. Indeed, the increase of the order of symmetry of the shape enhances the rate of *single* particle readsorption. This extends the time needed for a system to forget the initial configuration. However, the correlation curves do not differ qualitatively and they have similar shapes for all objects.

It is well known that the aging properties of the system are characterized by specific scaling properties of $C(t, t_w)$. For example, in the Tetris and Ising frustrated lattice gas models, it was found that the relaxation of $C(t, t_w)$ is given by the form [38]:

$$C(t, t_w) = (1 - c_\infty)\frac{\ln[(t_w + t_s)/\tau]}{\ln[(t + t_s)/\tau]} + c_\infty, \qquad (2)$$

where τ, t_s and c_∞ are fitting parameters. The above behavior is found in our model. In Fig. 6 we show the behavior of the correlation function $C(t, t_w)$ for objects (A), (B), and (C), when $P_d = 0.0015$. The waiting times t_w correspond to the
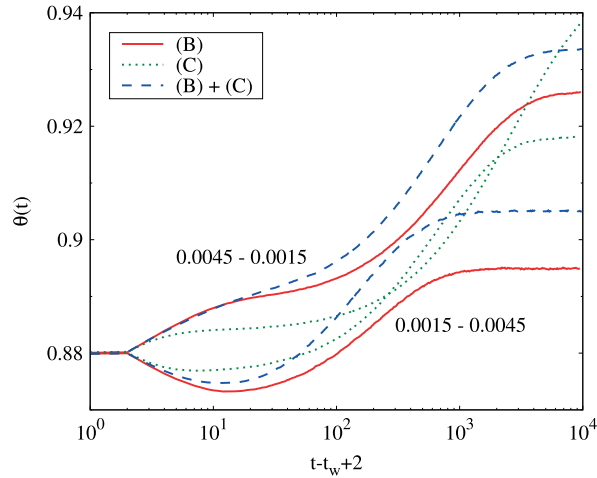
Fig. 9. Time evolution of coverage fraction $\theta^{(B)+(C)}$ for the mixture $(B) + (C)$ when the desorption probability is changed from $P_d^{(1)} = 0.0045$ to $P_d^{(2)} = 0.0015$ (from $P_d^{(1)} = 0.0015$ to $P_d^{(2)} = 0.0045$) at the time $t_w = 126$ ($t_w = 182$) needed for the system to reach the coverage $\theta_w^{(B)+(C)} = 0.88$, in the process of reversible RSA with $P_d^{(1)} = 0.0045$ ($P_d^{(1)} = 0.0015$). The time origin for each experiment has been taken at the time when the system reached the prescribed density θ_w.
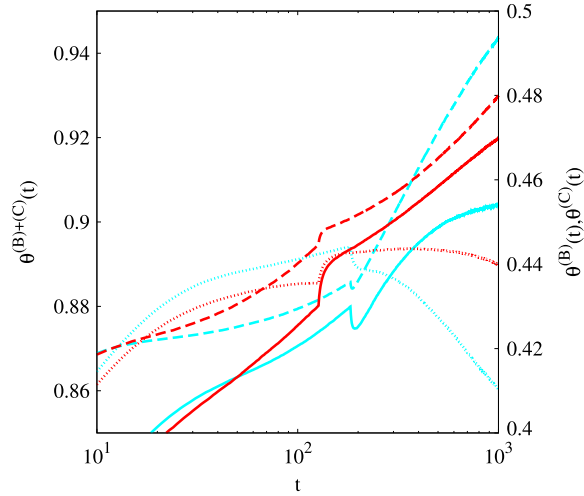
time needed for a system to reach the coverages $\theta_w = 0.87, 0.88, 0.89$. For all the shapes, the typical aging behavior is observed: the larger t_w, the longer memory of the initial state persists. The inset of Fig. 6 illustrates that when the two-time correlation function $C(t, t_w)$ is plotted as a function of $\ln[(t_w + t_s)/\tau]/\ln[(t + t_s)/\tau]$ the data for all three objects collapse onto single curve. This figure clearly demonstrates the existence of the single universal master function. It is interesting that the parameter t_s is equal for all objects, $t_s = 1760$. However, parameter τ depends on the shape: $\tau(A) = 81$, $\tau(B) = 210$, $\tau(C) = 43$. The shapes of higher order of symmetry n_s have lower values of scaling parameter τ.

3.1. Memory effects in mixtures

In the following, we shall investigate the role that the mixture composition and the symmetry properties of component shapes play in the deposition process. We shall mainly concentrate on the response of the reversible RSA model to sudden perturbations of the desorption probability P_d in the case of binary mixtures, composed of the shapes of different rotational symmetries but of the same number of segments.

Consider the two-component mixture of objects (B) and (C) with the symmetry axis of $n_s^{(B)} = 1$ and $n_s^{(C)} = 3$ order, respectively. The reversible RSA process for a binary mixture is as follows. From a large reservoir of shapes, that contains the shapes (B) and (C) with equal fractional concentrations, we choose one shape at random. We randomly select a lattice site and try to deposit the chosen shape in the same manner as in the case of the reversible RSA of pure depositing objects. Each adsorption attempt is followed by a desorption one with probability P_d. The quantity of interest is the fraction of total lattice sites, $\theta^{(B)+(C)}(t)$, covered by the deposited objects (B) and (C) at time t.

Fig. 7 shows the time dependence of the partial coverages $\theta^{(B)}(t)$ and $\theta^{(C)}(t)$ resulting from the reversible RSA of the binary mixture of (B) and (C) shapes, for two values of desorption probability, $P_d = 0.0045, 0.0015$. For shape (C) of higher order of symmetry $n_s^{(C)} = 3$, the partial coverage $\theta^{(C)}(t)$ is a monotonously increasing function of time and has the same general features as the coverage $\theta^{(B)+(C)}(t)$ for the mixture $(B) + (C)$. On the other hand, for shape (B) of lower order of symmetry $n_s^{(B)} = 1$, the partial coverage $\theta^{(B)}(t)$ is not monotonic in time. When the coverage $\theta^{(B)+(C)}(t)$ approaches to the coverage fraction that is equal to the jamming limit $\theta_J^{(B)+(C)} = 0.8624$, the partial coverage $\theta^{(B)}(t)$ reaches a broad maximum. This is followed by a slow relaxation of $\theta^{(B)}(t)$ to the smaller steady-state value $\theta_\infty^{(B)}$. At late enough time, when the coverage fraction is sufficient to make the geometry of the unoccupied sites complex, there is a strong dependence of the adsorption rate on the adsorbed shape [28,15]. Then, both rotational symmetry of the shapes and desorption events manage the single-particle readsorptions on the lattice and, eventually, allow replacements of the less symmetric particles by the more symmetric ones. This is reflected in the gradual decrease of the coverage fraction with time for the shape with the symmetry axis of lower order. Our results confirm that, for sufficiently high coverages of a mixture, the large times coverage fraction of more symmetric shapes exceeds the coverage fraction of less symmetric ones [31]. The steady-state value of the coverage fraction of the mixture components is always larger for the shapes with the symmetry axis of higher order n_s [31]. In Fig. 8 we compare the geometric status of the representative snapshots of patterns formed during the reversible deposition of mixture $(B) + (C)$. The snapshots are taken at the times t_w needed for the system to reach (a) the coverage $\theta^{(B)+(C)}(t_w) = 0.88$, and (b) the steady-state coverage $\theta_\infty^{(B)+(C)} = 0.9066$ in the process of reversible deposition with $P_d = 0.0045$. In Fig. 8(a) the partial coverage of triangles (C) ($\theta^{(C)}(t_w) = 0.4375$) is slightly smaller than that of angled

Fig. 10. Shown here is the response of the mixture $(B) + (C)$ to the desorption probability shift $P_d^{(1)} \rightarrow P_d^{(2)}$. Black (red) lines represent the results obtained for the abrupt change $P_d^{(1)} = 0.0045 \rightarrow P_d^{(2)} = 0.0015$ at the time t_w needed for the system to reach the coverage $\theta_w^{(B)+(C)} = 0.88$ in the process of reversible RSA with $P_d^{(1)} = 0.0045$. Grey (light blue) lines represent the results obtained for the abrupt change $P_d^{(1)} = 0.0015 \rightarrow P_d^{(2)} = 0.0045$ at the time t_w needed for the system to reach the coverage $\theta_w^{(B)+(C)} = 0.88$ in the process of reversible RSA with $P_d^{(1)} = 0.0015$. The solid lines represent the temporal behavior of the coverage fraction $\theta^{(B)+(C)}(t)$ (left-hand axis). The dashed and dotted lines are plotted against the right-hand axis and give the coverage fraction versus time t of the component shapes (C), $\theta^{(C)}(t)$ (dashed), and (B), $\theta^{(B)}(t)$ (dotted). (For interpretation of the references to color in this figure legend, the reader is referred to the web version of this article.)
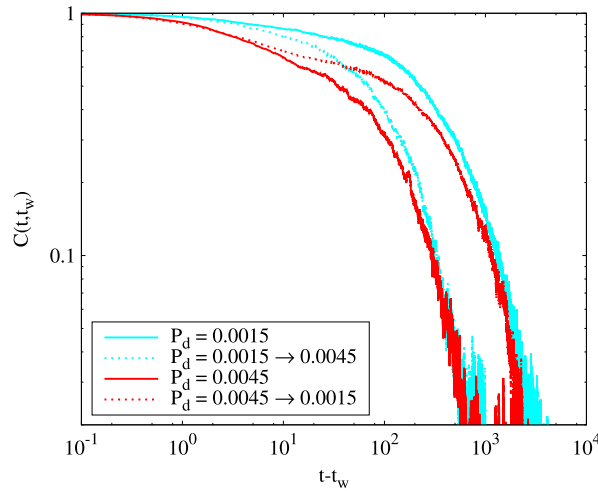
Fig. 11. Two-time density–density correlation function $C(t, t_w)$ for the mixture $(B) + (C)$, as a function of $t - t_w$. The waiting time t_w corresponds to the time needed for the system to reach the coverage $\theta_w^{(B)+(C)} = 0.88$. The solid lines represent the temporal behavior of $C(t, t_w)$ obtained for the fixed desorption probabilities $P_d = 0.0015$ and 0.0045, as indicated in the legend. The dashed lines represent the temporal dependence of $C(t, t_w)$ obtained from the runs during which an abrupt change of desorption probability $P_d^{(1)} = 0.0045 \rightarrow P_d^{(2)} = 0.0015$ ($P_d^{(1)} = 0.0015 \rightarrow P_d^{(2)} = 0.0045$) occurs at instant t_w, as indicated in the legend.

objects (B) ($\theta^{(B)}(t_w) = 0.4433$). However, at the steady-state density $\theta_\infty^{(B)+(C)} = 0.9066$ (Fig. 8(b)) the partial coverage fraction is larger for the shape with symmetry axis of higher order, i.e. $\theta_\infty^{(C)} = 0.5266 > \theta_\infty^{(B)} = 0.3800$.

Fig. 9 shows typical short-term memory effects after an abrupt change of the desorption probability P_d for the mixture $(B) + (C)$ and for pure component shapes, (B) and (C). Desorption probability P_d is switched from $P_d^{(1)} = 0.0045$ to $P_d^{(2)} = 0.0015$ and vice-versa, at the time t_w needed for a mixture to reach the coverage $\theta_w = 0.88$. Again, we observe that after several adsorption/desorption events the "anomalous" response ceases and there is a crossover to the "normal" behavior, with the relaxation rate becoming the same as in the constant forcing mode. However, it is interesting to note that during this transient stage, the temporal evolution of the total coverage fraction $\theta^{(B)+(C)}(t)$ is very similar to the one observed for the shape with the symmetry axis of lower order. Hence, the dynamics of the short-time response of the mixture $(B) + (C)$ to sudden perturbation of the desorption probability P_d is usually determined by the shape (B) of lower order of
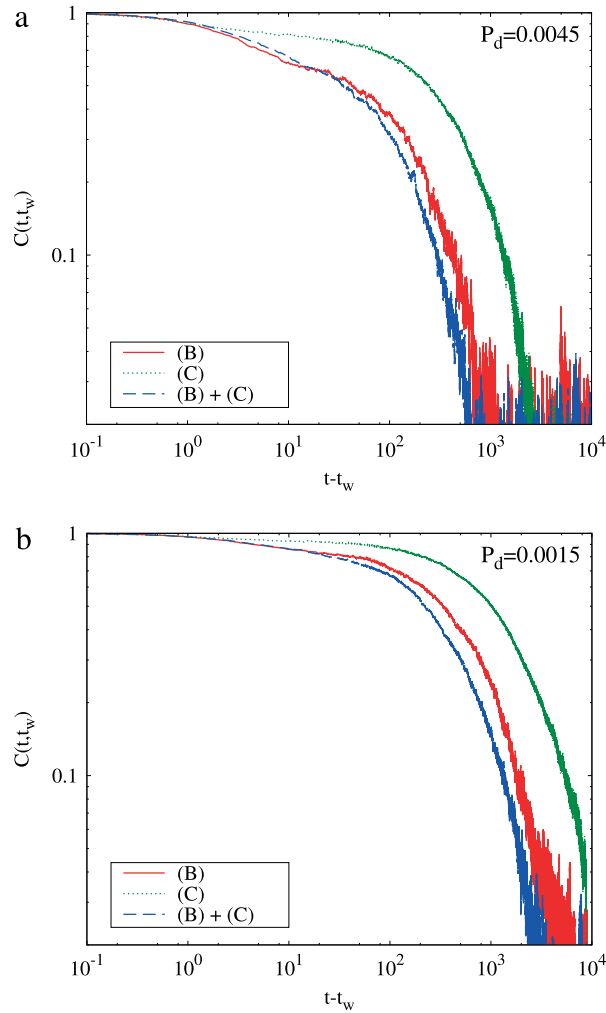
Fig. 12. Two-time density–density correlation function $C(t, t_w)$ for objects (B), (C), and mixture $(B) + (C)$, as a function of $t - t_w$. The waiting time t_w corresponds to the time needed for the system to reach the coverage $\theta_w = 0.88$ when the desorption probability has the constant values (a) $P_d^{(1)} = 0.0045$, and (b) $P_d^{(1)} = 0.0015$.

symmetry, $n_s^{(B)} = 1$. Fig. 10 puts into evidence the temporal behavior of the partial coverage fraction for component shapes (B) and (C) during the transient time. As in the case of pure lattice shapes, we observe that the change in the compaction rate on short-time scales is less pronounced for the component shape of higher symmetry order.

In Fig. 11 we show the temporal dependence of $C(t, t_w)$ (see, Eq. (1)) for the mixture $(B) + (C)$, when the waiting time t_w corresponds to the time needed for a system to reach the coverage $\theta_w^{(B)+(C)} = 0.88$. Correlation function $C(t, t_w)$ is displayed both for the fixed desorption probabilities, $P_d = 0.0015, 0.0045$, and for the cases with abrupt changes of desorption probability $P_d^{(1)} = 0.0045 \rightarrow P_d^{(2)} = 0.0015$, and $P_d^{(1)} = 0.0015 \rightarrow P_d^{(2)} = 0.0045$ at instant t_w. As for the pure lattice shapes, correlation functions calculated for the mixture $(B) + (C)$ in the case of perturbed systems $(\Delta P_d = P_d^{(1)} - P_d^{(2)} \lessgtr 0)$ interpolates between the two correlation functions obtained for the systems with constant desorption probabilities $P_d^{(1)}$, and $P_d^{(2)}$.

It is instructive to compare the temporal behavior of the correlation function $C(t, t_w)$ for the mixture with results for $C(t, t_w)$ in the case of reversible deposition of pure component shapes. In Fig. 12 we show the time evolution of $C(t, t_w)$ during the deposition of objects (B), (C), and the mixture $(B) + (C)$, for the waiting time t_w needed for a system to reach the coverage $\theta_w = 0.88$ when the desorption probability has the constant values $P_d^{(1)} = 0.0045$ (Fig. 12(a)) and $P_d^{(1)} = 0.0015$ (Fig. 12(b)). We can clearly see that for short times, $C(t, t_w)$ for the mixture $(B) + (C)$ decays in a similar way as for shape (B) with the symmetry axis of lower order, $n_s^{(B)} = 1$. This changes slightly at intermediate times, when the correlation function $C(t, t_w)$ for the mixture starts to decay faster than the density correlations of component shapes. Hence, we observe the weakening of correlation features in multicomponent systems.

4. Conclusions

Along this paper, we have studied the nonequilibrium response of reversible RSA model to an instantaneous change in the value of desorption probability P_d. We have performed extensive simulations of reversible deposition using objects of different rotational symmetries on a triangular lattice. The shapes are made by self-avoiding lattice steps. First, it was shown that the change in the compaction rate has opposite sign than that of the modification of the desorption probability P_d, in contrast with the long-time behavior, where the relaxation is faster for larger P_d. These results are in a qualitative agreement with the observations in experiments on granular compaction [25]. Further, our numerical simulations have shown that the short-time response to an instantaneous change in the desorption probability P_d strongly depends on the symmetry properties of the shapes. We have found that the dynamical behavior is severely slowed down with the increase of the order of symmetry of the shape. When the desorption probability P_d is suddenly decreased/increased, compaction/decompaction rate of the perturbed system on short-time scales is larger for shapes with symmetry axis of lower order. We have also pointed out the importance of collective events for governing the short-time coverage behavior of shapes with different rotational symmetry.

We have also considered the nonequilibrium two-time density–density correlation function $C(t, t_w)$. We have observed that decay of the correlation function $C(t, t_w)$ depends on the order of symmetry axis of the shape n_s. It was confirmed that the density correlation decays slower for more symmetrical shapes. Eq. (2) states that, for the long enough times, the correlation $C(t, t_w)$ is a function of the ratio $\ln(t_w)/\ln(t)$. Such scaling behavior is in agreement with the Ising frustrated lattice gas model and the Tetris model [38], but in contrast with the parking lot model [27], for which a t/t_w behavior has been observed.

Special attention has been paid to the mixtures containing objects of various shapes, but made of the same number of segments. It was found that the dynamics of the short-time response of the mixture to sudden perturbation of the desorption probability P_d is determined by the shape of lower order of symmetry. In addition, our results confirm the weakening of correlation features for the deposition processes in multicomponent systems.

Acknowledgments

References

[1] P.J. Flory, Intramolecular reaction between neighboring substituents of vinyl polymers, J. Am. Chem. Soc. 61 (1939) 1518.
[2] J.W. Evans, Random and cooperative sequential adsorption, Rev. Modern Phys. 65 (1993) 1281–1329.
[3] V. Privman, Dynamics of nonequilibrium deposition, Colloids Surf. A 165 (2000) 231–240.
[4] A. Cadilhe, N.A.M. Araújo, V. Privman, Random sequential adsorption: from continuum to lattice and pre-patterned substrates, J. Phys.: Condens. Matter 19 (2007) 065124.
[5] V. Privman (Ed.), Nonequilibrium Statistical Mechanics in One Dimension, Cambridge University Press, Cambridge, UK, 1997.
[6] B. Senger, J.C. Voegel, P. Schaaf, Irreversible adsorption of colloidal particles on solid substrates, Colloids Surf. 165 (2000) 255–285.
[7] J. Talbot, G. Tarjus, P.R. Van Tassel, P. Viot, From car parking to protein adsorption: an overview of sequential adsorption processes, Colloids Surf. A 165 (2000) 287–324.
[8] J.J. Ramsden, G.I. Bachmanova, A.I. Archakov, Kinetic evidence for protein clustering at a surface, Phys. Rev. E 50 (1994) 5072.
[9] J. Talbot, G. Tarjus, P. Viot, Adsorption–desorption model and its application to vibrated granular materials, Phys. Rev. E 61 (2000) 5429–5438.
[10] Lj. Budinski-Petković, S.B. Vrhovac, Memory effects in vibrated granular systems: Response properties in the generalized random sequential adsorption model, Eur. Phys. J. E 16 (2005) 89–96.
[11] R.S. Ghaskadvi, M. Dennin, Reversible random sequential adsorption of dimers on a triangular lattice, Phys. Rev. E 61 (2000) 1232–1238.
[12] E. Frey, A. Vilfan, Anomalous relaxation kinetics of biological latticeligand binding models, Chem. Phys. 284 (2002) 287.
[13] P.L. Krapivsky, E. Ben-Naim, Collective properties of adsorption–desorption processes, J. Chem. Phys. 100 (1994) 6778–6782.
[14] Lj. Budinski-Petković, U. Kozmidis-Luburić, Adsorption–desorption processes of extended objects on a square lattice, Physica A 301 (2001) 174.
[15] Lj. Budinski-Petković, M. Petković, Z.M. Jakšić, S.B. Vrhovac, Symmetry effects in reversible random sequential adsorption on triangular lattice, Phys. Rev. E 72 (2005) 046118.
[16] I. Lončarević, Lj. Budinski-Petković, S.B. Vrhovac, A. Belić, Adsorption, desorption, and diffusion of k-mers on a one-dimensional lattice, Phys. Rev. E 80 (2009) 021115.
[17] G. Tarjus, P. Viot, Statistical mechanical description of the parking-lot model for vibrated granular materials, Phys. Rev. E 69 (2004) 011307.
[18] J.B. Knight, C.G. Fandrich, C.N. Lau, H.M. Jaeger, S.R. Nagel, Density relaxation in a vibrated granular material, Phys. Rev. E 51 (1995) 3957–3963.
[19] F.X. Villarruel, B.E. Lauderdale, D.M. Mueth, H.M. Jaeger, Compaction of rods: Relaxation and ordering in a vibrated, anisotropic granular material, Phys. Rev. E 61 (2000) 6914–6921.
[20] P. Philippe, D. Bideau, Compaction dynamics of granular medium under vertical tapping, Europhys. Lett. 60 (2002) 677.
[21] P. Ribière, P. Richard, D. Bideau, R. Delannay, Experimental compaction of anisotropic granular media, Eur. Phys. J. E 16 (2005) 415–420.
[22] P. Richard, M. Nicodemi, R. Delannay, P. Ribière, D. Bideau, Slow relaxation and compaction of granular systems, Nature Mater. 4 (2005) 121–128.
[23] P. Ribière, P. Richard, P. Philippe, D. Bideau, R. Delannay, On the existence of stationary states during granular compaction, Eur. Phys. J. E 22 (2007) 249–253.
[24] A.J. Kolan, E.R. Nowak, A.V. Tkachenko, Glassy behavior of the parking lot model, Phys. Rev. E 59 (1999) 3094–3099.
[25] C. Josserand, A. Tkachenko, D.M. Mueth, H.M. Jaeger, Memory effects in granular materials, Phys. Rev. Lett. 85 (2000) 3632–3635.
[26] M. Nicolas, P. Duru, O. Pouliquen, Compaction of a granular material under cyclic shear, Eur. Phys. J. E 3 (2000) 309–314.
[27] J. Talbot, G. Tarjus, P. Viot, Aging and response properties in the parking-lot model, Eur. Phys. J. E 5 (2001) 445–449.
[28] Lj. Budinski-Petković, U. Kozmidis-Luburić, Random sequential adsorption on a triangular lattice, Phys. Rev. E 56 (1997) 6904.
[29] Lj. Budinski-Petković, S.B. Vrhovac, I. Lončarević, Random sequential adsorption of polydisperse mixtures on discrete substrates, Phys. Rev. E 78 (2008) 061603.

[30] D. Dujak, I. Lončarević, Lj. Budinski-Petković, S.B. Vrhovac, A. Karač, Adsorption–desorption processes of polydisperse mixtures on a triangular lattice, Phys. Rev. E 91 (2015) 032414. http://dx.doi.org/10.1103/PhysRevE.91.032414.
[31] I. Lončarević, Lj. Budinski-Petković, S.B. Vrhovac, Reversible random sequential adsorption of mixtures on a triangular lattice, Phys. Rev. E 76 (2007) 031104.
[32] S. Živković, Z.M. Jakšić, I. Lončarević, Lj. Budinski-Petković, S.B. Vrhovac, A. Belić, Optimization of the monolayer growth in adsorption–desorption processes, Phys. Rev. E 88 (2013) 052131. http://dx.doi.org/10.1103/PhysRevE.88.052131.
[33] Lj. Budinski-Petković, U. Kozmidis-Luburić, A. Mihailović, Random sequential adsorption with diffusional relaxation on a square lattice, Physica A 293 (2001) 339.
[34] Lj. Budinski-Petković, T. Tošić, Adsorption, desorption and diffusion of extended objects on a square lattice, Physica A 329 (2003) 350.
[35] P. Ranjith, J.F. Marko, Filling of the one-dimensional lattice by *k*-mers proceeds via fast power-law-like kinetics, Phys. Rev. E 74 (2006) 041602.
[36] S.S. Manna, N.M. Švrakić, Random sequential adsorption: line segments on the square lattice, J. Phys. A: Math. Gen. 24 (1991) L671–L676.
[37] J. Talbot, G. Tarjus, P. Viot, Sluggish kinetics in the parking lot model, J. Phys. A: Math. Gen. 32 (1999) 2997–3003.
[38] M. Nicodemi, A. Coniglio, Aging in out-of-equilibrium dynamics of models for granular media, Phys. Rev. Lett. 82 (1999) 916–919.